Biochemistry

 Volume 37, Number 22 June 2, 1998

Accelerated Publications

Protein Farnesyltransferase: Structure and Implications for Substrate Binding

Pete Dunten,* Ursula Kammlott, Robert Crowther, David Weber, Robert Palermo, and Jens Birktoft

Roche Research Center, Hoffmann-La Roche Inc., 340 Kingsland, Building 76, Nutley, New Jersey 07110

Received March 6, 1998; Revised Manuscript Received April 6, 1998

ABSTRACT: The rat protein farnesyltransferase crystal structure has been solved by multiple isomorphous replacement methods at a resolution of 2.75 Å. The three-dimensional structure, together with recent data on the effects of several mutations, led us to propose a model for substrate binding which differs from the model presented by Park et al. based on their independent structure determination [Park, H.-W., Boduluri, S. R., Moomaw, J. F., Casey, P. J., and Beese, L. S. (1997) *Science 275*, 1800−1804]. Both farnesyl diphosphate and peptide substrates can be accommodated in the hydrophobic active-site barrel, with the sole charged residue inside the barrel, Arg202 of the β-subunit, forming a salt bridge with the negatively charged carboxy terminus of peptide substrates. Our proposals are based in part on the observation of electron density in the active site which can be modeled as bound farnesyl diphosphate carried through the enzyme purification. In addition, our model explains in structural terms the results of mutational studies which have identified several residues critical for substrate specificity and catalysis.

The enzyme protein farnesyltransferase has been the subject of anticancer research aimed at interfering with Ras function (*1*). Activated Ras is found in association with 25% of all human cancers, and Ras function requires membrane localization. A series of steps modifies the C-terminus of Ras, converting it to a hydrophobic membrane anchor. The enzyme protein farnesyltransferase (Ftase)[1] catalyzes the first of these steps by transferring the farnesyl group from farnesyl diphosphate to the cysteine side chain in the CAAX sequence motif at the C-terminus of Ras. (The CAAX motif consists of Cys followed by two aliphatic residues and an uncharged residue "X" at the C-terminus.) After farnesylation, the final three amino acid residues are proteolytically removed from the C-terminus of Ras and the newly exposed cysteine carboxylate is methyl esterified, leaving a hydrophobic farnesylcysteine tail. The hydrophobic tail is subsequently inserted in the membrane, leading to the membrane localization of Ras.

The human Ftase is a heterodimer consisting of a 379-residue α-subunit and 437-residue zinc-containing β-subunit. The α-subunit is also a component of the heterodimeric type I protein geranylgeranyltranferase (GGtase), an enzyme which transfers the geranylgeranyl group from geranylgeranyl diphosphate to the cysteine in the C-terminal CAAX sequence of Gγ, RhoB, and Rac proteins. The two enzymes discriminate on the basis of the C-terminal residue in the CAAX sequence: Ftase acts preferentially on substrates with Met, Gln, Ser, Ala, or Cys, while the type I GGtase prefers substrates with Leu or Phe at the final position.

Elucidation of the three-dimensional structure of one of these important enzymes would accelerate the search for specific inhibitors with potential value as anticancer agents, as well as help in understanding the enzyme's substrate specificity and mechanism of action. In fact, several structures will be required for a full understanding of the protein's function, given the possibility of formation of

[1] Abbreviations: FPP, farnesyl diphosphate; Ftase, protein farnesyltransferase; GGtase, protein geranylgeranyltransferase; MIR, multiple isomorphous replacement; SIR, single isomorphous replacement.

S0006-2960(98)00531-5 CCC: $15.00
Published on Web 05/07/1998

complexes with peptide and/or farnesyl diphosphate substrates as well as with inhibitors. Park et al. succeeded in determining the crystal structure of the full-length rat enzyme, with the active site occluded by crystal packing interactions (*2*). We report here the independent MIR solution of a new crystal form of a truncated version of Ftase and an analysis of the structure in terms of the enzyme's function.

The structure sheds light on the results of mutagenesis studies of the enzyme which have either targeted conserved residues or screened for random mutations conferring activity against variants of the CAAX sequence. The mutagenesis results mapped onto the three-dimensional structure define regions of the enzyme involved in binding the two substrates, the CAAX motif of Ras and farnesyl diphosphate (FPP). Our observation of residual electron density in the active site suggests FPP copurified with Ftase, and the location of the density supports the conclusions reached by the mutagenesis studies. Taken together, these results suggest an alternative model for substrate binding to that proposed by Park et al.

METHODS

Protein Expression and Purification. Recombinant baculovirus expression vectors for both the α- and β-subunits of rat Ftase were a gift of Drs. M. S. Brown and J. L. Goldstein (Southwestern Medical Center, Dallas, TX). The expression in High Five cells (Invitrogen) was carried out as described (*3*), with cell harvest 48 h after infection. Harvested cells were stored at −80 °C.

Frozen cells were thawed in 50 mM Tris·HCl, 100 mM NaCl, 20 μM $ZnCl_2$, and 1 mM DTT, pH 7.4, and lysed in a Parr extraction bomb pressurized to 1000 psi. Particulate material was removed from the crude extract by centrifugation at ∼50000*g* for 45 min. The extract was applied to a column of Q-Sepharose equilibrated in 50 mM Tris·HCl, 50 mM NaCl, 20 μM $ZnCl_2$, and 1 mM DTT, pH 7.4, and proteins were eluted with a gradient from 0.05 to 0.5 M NaCl. Fractions containing Ftase were pooled and brought to 1.2 M KCl and then applied to a column of phenyl-Sepharose equilibrated in 20 mM Tris·HCl, 10 μM $ZnCl_2$, 1 mM DTT, and 1.5 M KCl, pH 8.0; proteins were eluted by applying a gradient from 1.5 to 0 M KCl. Fractions containing Ftase were again pooled and concentrated, and the material was gel filtered on a column of Superdex 200 equilibrated in 50 mM Tris·HCl, 150 mM NaCl, 10 μM $ZnCl_2$, 0.1% octyl β-glucoside, 1 mM DTT, and pH 8.0. The peak containing Ftase was collected and loaded on a MonoQ column equilibrated in 50 mM Tris·HCl, 100 mM NaCl, 20 μM $ZnCl_2$, 0.1% octyl β-glucoside, 1 mM DTT, and pH 7.5. Proteins were eluted by applying a gradient from 0.1 to 0.6 M NaCl. All steps in the purification prior to the MonoQ chromatography were carried out at 4 °C. Enzyme activity was measured using the Amersham [^{3}H]SPA reagents. The yield of Ftase was approximately 1 mg/gram of cells. N-Terminal sequencing showed that some proteolysis occurs during the fermentation, removing either the first 8 or 15 residues of the β-subunit.

Crystallization screens with Ftase alone as well as in complex with a number of inhibitors were conducted using the Hampton Research Crystal Screen kits I and II. At best only tiny, unsuitable crystals were obtained. To generate a new protein form, several proteases were screened with the goal of removing the proline-rich sequence from the N-terminus of the α-subunit. Treatment with protease GluC from *Staphylococcus aureus* was found to decrease the α-subunit's apparent M_r from 43 000 to 35 000. Purified Ftase was incubated with GluC at a protease to substrate ratio of 1:100 for 1 h at room temperature, at which time the digestion was stopped by addition of 3,4-dichloroisocoumarin to a final concentration of 0.1 mM. N-Terminal protein sequencing showed that the protease cleaved the α-subunit after Glu45α. Partial peptide mapping with mass spectral analysis indicated the protease also cleaved the β-subunit near its C-terminus, after Glu425β.

Crystallization and Data Collection. Crystallization conditions for the truncated Ftase were established using the Hampton Research screens and the hanging drop method. The inhibitor BG168, *N*-acetyl-D-seryl-L-cysteinyl-L-phenylglycyl-L-isoleucyl-L-methionine, was a gift of Dr. J. Marsters (Genentech). Protein and inhibitor were combined at final concentrations of 20 mg/mL enzyme and 1 mM compound in a buffer of 20 mM Tris·HCl, 10 mM NaCl, 20 μM $ZnCl_2$, and 10 mM DTT, pH 7.5. The protein stock and an equal volume of precipitant (0.4 M $NH_4H_2PO_4$, 10 mM DTT, pH 4.4) were mixed and equilibrated at 4 °C over a reservoir containing precipitant. Routine success in growing crystals could be achieved if the drops were seeded with a dilute stock of seeds made from crushed crystals. For data collection, crystals were transferred to a cryoprotectant consisting of 30% PEG400 and 1 M NaOAc, pH 4.5, before flash-freezing in a stream of nitrogen gas at −184 °C. Heavy-atom derivative soaks were performed in the cryobuffer. The K_3IrCl_6 soak was for 6 h at a concentration of 1 mM heavy-atom reagent.

Native and derivative data sets were collected using a Rigaku rotating anode generator equipped with focusing optics from Charles Supper and a 30 cm MAR imaging plate. A high-resolution native data set was collected from a frozen crystal on a 30 cm MAR imaging plate at NSLS beamline X12-B using radiation of wavelength 0.978 Å. All data sets were processed with the programs DENZO and SCALEPACK (*4*).

The crystals have unit cell parameters $a = b = 170.0$ Å and $c = 68.9$ Å, and their diffraction pattern is consistent with space group $P6_1$. With one α/β heterodimer per asymmetric unit, the solvent content is estimated to be 59%.

Structure Solution and Refinement. Three heavy-atom sites were identified using the program RSPS (*5*) to interpret the $IrCl_6$ difference Patterson map. After additional sites of lower occupancy were identified using the phases calculated from the first three sites, the SIR phases were improved by application of solvent flattening and histogram matching in the program DM (*5*). The highest feature in the resulting electron density map (a peak of 7.1σ) was tentatively assigned to the Zn atom of the β-subunit. A second derivative was obtained by soaking a crystal for 2 days in cryobuffer containing 1 mM EDTA. The difference Patterson for the EDTA "derivative" yielded a solution with a single site at the anticipated location of the Zn atom. MIR phases were calculated on the basis of the two derivatives, and after solvent flattening and histogram matching, an electron density map was calculated at 3.1 Å resolution. The density for the helical core of the β-subunit was easily interpretable, and the fold of the α-subunit was obvious after

Table 1: Refinement Statistics

resolution limits	12−2.75 Å
no. of reflections	28142
% complete	95.7% (86.3%)[a]
R-sym	6.4% (15.0%)[a]
no. of protein atoms	5836
R-factor[b]	24.6%
R-free[b]	30.8%
Procheck overall *G*-value[c]	+0.13

[a] 2.85−2.75 Å. [b] No solvent atoms included. [c] Positive values indicate better than average stereochemistry, in comparison with other structures determined at the same resolution.

inspection of the score map produced by the program ESSENS using a five-residue α-helix as search model (*6*). A model was built into the density using O (*7*), and the map was updated during the model building process by combining the MIR and model phases with SIGMAA (*5*). After 500 residues were built into the density, several loops were missing, and the remaining features of the map were not readily interpreted. A new set of phases was calculated using the program SHARP (*8*), starting with the native and derivative data sets and making no use of the partial Ftase model. After these phases were improved via solvent flipping in SHARP [a procedure which utilizes the program SOLOMON (*5*)], an electron density map was calculated. This map was much clearer and facilitated completion of the model. The correctness of the tracing was checked by calculating a map with phases from the model and $F^+ - F^-$ amplitudes from the native data collected with 1.54 Å radiation. Peaks were present at the locations of the zinc and 26 of the 28 sulfur atoms in the structure. The two exceptions are both Met residues whose side chains extend into solvent. The model includes 315 of the 332 residues in the truncated α-subunit, 400 of the 410 residues in the truncated β-subunit, and the catalytic zinc atom.

The initial *R*-factor for data in the 12.5−3.1 Å resolution range was 47.6% (*R*-free 48.1%, based on 10% of the data). Cycles of rebuilding and refinement in REFMAC (*5, 9*) lowered the *R*-factor to 26.7% (*R*-free 34.0%), after which the high-resolution limit was extended to 2.75 Å. Rebuilding made use of $F_o - F_c$, $2F_o - F_c$, and simulated annealing omit maps calculated by X-PLOR (*10*). The model's geometry was critically evaluated using features of O, PROCHECK (*11*), PROMOTIF (*12*), and WHAT-IF (*13*). The current refinement statistics are given in Table 1.

RESULTS AND DISCUSSION

Structure Determination. Crystals of protein farnesyltransferase were obtained from Ftase treated with the protease GluC. GluC digestion removes the proline-rich sequence at the N-terminus of the α-subunit as well as 12 residues from the C-terminus of the β-subunit without inactivating the enzyme. The structure was determined via MIR using two derivatives and native data to 2.75 Å resolution. Somewhat surprisingly, removal of the single Zn from the enzyme by soaking a crystal in EDTA yielded a useful derivative. Both subunits are α-helical folds, and the α-helices were easily recognized in the MIR electron density map by the automated search algorithm in the program ESSENS (*6*). The model includes residues 55−369 of the truncated α-subunit and residues 22−421 of the truncated β-subunit. Residues 46−54 and 370−377 are missing from the truncated α-subunit, as are residues 16−21 and 422−425 from the truncated β-subunit. The current *R*-factor is 24.6%, with *R*-free 30.8%.

Though the peptide inhibitor BG168 was present during the growth of the crystals used for the structure determination, we do not see clear density for the inhibitor in our structure. The density present in the active-site cavity could not be successfully modeled as BG168. In particular, the density does not fit well to the three prominent side chains at the C-terminus of BG168, phenylglycine, isoleucine, and methionine. After the X-ray data used to solve the structure were collected, crystals were subsequently obtained from inhibitor-free protein, using the same crystallization conditions as for the BG168-inhibited enzyme. Thus it is clear in retrospect that inhibitors are not required for the growth of crystals. The absence of any clear density for the peptide inhibitor is probably due to the fact that the crystals were grown at a pH where farnesyltransferase has little affinity for peptides [farnesyltransferase can be eluted from a CAAX peptide-affinity resin by lowering the pH from neutrality to pH 5 (*14*)].

Structure. As shown in Figure 1, the α-subunit is a right-handed superhelix based on seven copies of a helix−turn−helix repeat. Toward the end of the refinement of the structure, a 7σ peak in the $F_o - F_c$ map near Ser93 of the α-subunit was modeled as a bound phosphate ion (Figure 1). The α-subunit of the human farnesyltransferase has been shown to be phosphorylated by the type I TGF-β receptor, and the phosphorylation has been suggested to serve a regulatory purpose (*15*−*17*). Residue 93α is Ser in three mammalian farnesyltransferase sequences and Thr in the yeast enzyme. The bound sulfate is located near the N-terminus of the first α-helix in the α-subunit, where the helix dipole interacts favorably with anions. By analogy to the case of glycogen phosphorylase *b*, where a bound sulfate ion in the crystal structure "marked" the site of phosphorylation by phosphorylase kinase, it seems reasonable to suggest that Ser93α might be phosphorylated by the type I TGF-β receptor. As residue 93α is near both the α/β subunit interface and the active site, phosphorylation at this site could directly alter either the quaternary structure of the enzyme or the binding of substrates and thereby regulate the enzyme's activity.

The β-subunit is an α-helical barrel open at one end and plugged at the other by a turn in the chain at residues 398−402 near the C-terminus. The active-site Zn is located on the inside of the barrel near its upper end, where it is coordinated by the side chains of Asp297β, Cys299β, and His362β. The other notable feature of the barrel is its hydrophobic interior surface: the hydrophobic character of the active site fits well with the hydrophobic nature of both farnesyl diphosphate and peptides such as CVIM. The sequence differences between the rat and human Ftases all map on the surface of the enzyme away from the active-site Zn and interior of the barrel. This fact, together with the observation that the rat and human enzymes are closely related, with 93% identity over 379 residues for the α-subunits and 97% identity over 437 residues for the β-subunits, suggests that the structure of the rat enzyme will be useful for drug design efforts.

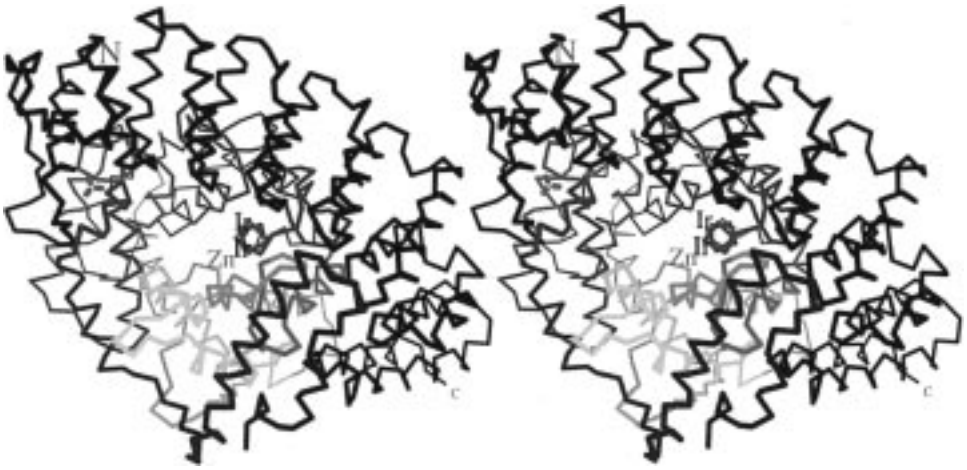

FIGURE 1: Stereoview looking into the active site. The α-chain is shown in black with N- and C-termini labeled, and the *β*-chain is color-ramped from blue at the N-terminus to orange at the C-terminus. The adventitiously bound phosphate ion is shown in ball-and-stick form. The locations of the catalytic zinc and the anion binding sites occupied by $IrCl_6$ ions are indicated.

Although a detailed comparison with the independent structure determined by Park et al. (*2*) is not possible without access to the atomic coordinates, there appear to be no gross differences between the two structures. The calculated surface area buried at the α/*β* subunit interface is within 5% of 3300 Å^2 for the two structures, which suggests that the association of the α- and *β*-subunits is very similar, if not identical, in the two crystal forms. The packing between molecules in the two crystals differs, as described further below.

Substrate Binding. The α-subunit contacts the *β*-subunit barrel around half its circumference at the upper, open end of the barrel (Figure 1). This arrangement places several residues from the α-subunit near the active-site Zn. In particular, the side chains of Lys164α and His201α contribute to the formation of two anion binding sites 6.7 and 7.5 Å from the Zn. His248*β*, Lys294*β*, Lys353*β*, Lys356*β*, and Arg291*β* also contribute to the formation of the two sites, which were occupied by $IrCl_6$ ions in the heavy-atom derivative crystal used to solve the structure (Figure 2). The proximity of these sites to the active-site Zn and their highly charged character suggest that they represent part of the binding site for the diphosphate moiety of the substrate farnesyl diphosphate. The involvement of residues from both subunits is consistent with the observation that neither subunit alone is capable of binding FPP (*18*). Thus both subunits would appear to have a role in binding and orienting the leaving group of FPP appropriately for catalysis.

Support for the proposal that the $IrCl_6$ ions occupy the diphosphate binding site can be found in a recent mutagenesis study of the yeast enzyme. Several highly conserved residues in the *β*-subunit were altered via site-directed mutagenesis, and the kinetic constants of the mutant enzymes were determined (*19*). The change with the most dramatic effect on the apparent K_M for FPP was replacement of Glu256*β* with Ala, which raised K_M(FPP) over 100-fold. The corresponding residue in the rat enzyme, Glu246*β*, is almost completely inaccessible to solvent but helps to fix the side chain of Arg291*β* adjacent to the position of one of the $IrCl_6$ ions (Figure 2). An extensive set of interactions orients the side chain of Arg291*β*: the side chain of Glu246*β* interacts with that of Arg291*β* as well as with the side chains of Asn234α and Ser235α, and the main chain oxygen of

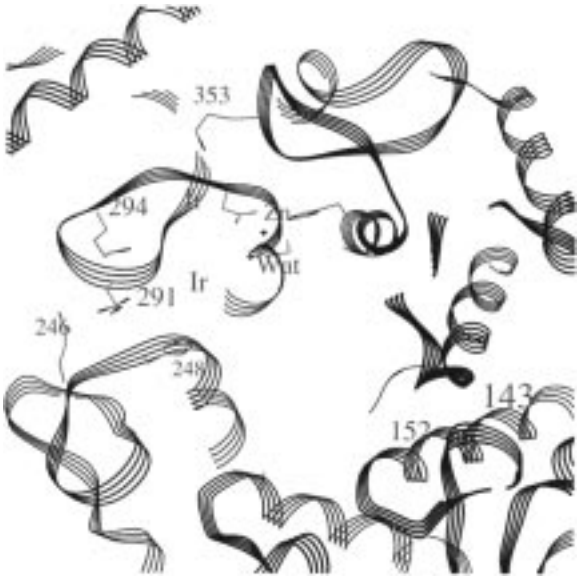

FIGURE 2: Proposed location of the diphosphate of FPP (Ir sites) relative to the active-site zinc. Side chains involved in forming the sites are labeled. Residues colored red on the opposite side of the active-site cavity are implicated in peptide binding by mutagenesis studies. The α-chain has been omitted for purposes of clarity.

Lys198α is within H-bonding distance of NH1 of Arg291*β*. Proper formation of the proposed FPP binding site thus depends on interactions between the α- and *β*-subunits of farnesyltransferase. Dolence et al. also replaced the yeast equivalent of Arg291*β* with Gln and measured a 2-fold increase in the apparent K_M for FPP. K_{cat} for the Arg291*β* to Gln mutant enzyme was reduced 20-fold relative to the wild type. While the Gln amide might substitute for Arg in FPP binding, it would not provide the same amount of stabilization to any charge developing on the leaving oxygen of the diphosphate moiety of FPP during catalysis.

The residual electron density in the hydrophobic pocket (Figure 3) can be modeled as farnesyl diphosphate, with the hydrophobic farnesyl tail in van der Waals contact with residues of the *β*-subunit lining one side of the pocket. The location of the diphosphate moiety is not expected to reflect the mode of binding during catalysis, as there was no Mg^{2+} present in the crystallization medium. The *B*-factor for the bound ligand is consistent with partial, rather than full,

FIGURE 3: Stereoview of the residual $F_o - F_c$ density in the active site contoured at the 1σ level. The model of farnesyl diphosphate fit to the density is shown in green with red oxygen atoms; the terminal phosphate can be placed in either of two locations (not shown). The labeled residues buried by FPP binding are Cys254β and Trp303β. The labeled residues thought to be involved in interactions with the C-terminal residue of the peptide substrate are Pro152β and Arg202β.

occupancy of the active site. Although no FPP was added during the crystallization, its presence is not surprising considering the tight binding constant [K_d ~10 nM (*18*, *20*)] and the fact that the purification protocol was not designed to strip bound ligands from the enzyme. In the model, the farnesyl moiety makes van der Waals contact with the aliphatic part of Arg202β's side chain, the C_α of Gly250β, and the side chain of Trp303β. Binding of FPP effectively buries residues Tyr205β and Cys254β at the bottom of the pocket. The bound FPP does not completely fill the hydrophobic interior of the active-site barrel in our model. Arg202β and the residues implicated by mutagenesis as being involved in peptide binding line the space left unoccupied after FPP binding (see below). The structural results suggest an explanation for the known requirement for FPP to bind first prior to catalytic turnover (*20*, *21*). By filling only part of the active-site barrel and buttressing Arg202β, FPP itself plays a role in orienting the peptide substrate for catalysis.

The results of genetic experiments implicate a small set of residues as being involved in discriminating between substrates which differ at the final position of the CAAX sequence motif. Tamanoi's group looked for mutations in the yeast Ftase which would change its substrate specificity toward that of the type I GGtase (*22*, *23*). GGtase prefers protein substrates with the sequence CAAL at the C-terminus, while Ftase is most active on substrates with Met, Gln, Ser, Ala, or Cys at the C-terminal position. Rine's group identified mutations in the yeast Ftase which enabled the enzyme to farnesylate substrates with a charged residue at the C-terminus (*24*). The residues identified via genetic methods correspond to Gly143β, Pro152β, Tyr361β, and Tyr365β of the rat enzyme and are all located along one side of the hydrophobic pocket in the center of the β-subunit barrel. The residues implicated by the genetic screens as being involved in peptide binding are all located on the face of the barrel opposite the bound FPP in our model, supporting our interpretation of the electron density (Figure 3). Pro152β, one of the residues identified in the genetic screens for mutants which farnesylate substrates ending with CAAL, is near the side chain of Arg202β in the X-ray structure. The location of the mutated residues in relation to Arg202β suggests that Arg202β interacts with the C-terminal carboxylate of the peptide substrate, forming a salt bridge to neutralize its charge. Arg202β is conserved in all Ftase and GGtase sequences, as would be expected if it played a role in binding the C-terminal carboxylate of peptide substrates. The distance separating the solvent molecule occupying the open coordination position at the active-site Zn and NH1 of Arg202β is 12.5 Å. If a tetrapeptide such as CVIM were to bridge this distance, with the Cys sulfur in the position of the solvent coordinating the active-site Zn, then the peptide would have to adopt an extended conformation in order to place the C-terminal carboxylate adjacent to the guanido group of Arg202β. An extended conformation for the bound peptide has been proposed earler, based on a series of peptidomimetic inhibitors with a Cys and Met separated by a variable spacer. The optimal distance separating the sulfur and carboxylate in that series of peptidomimetic inhibitors with restricted conformational flexibility was found to be 10.5 Å, with an IC_{50} for inhibition of Ftase activity in the 50−100 nM range (*25*, *26*).

In the crystals obtained by Park et al., the C-terminus of the β-chain of one molecule reaches into the active site of a neighboring molecule in the crystal lattice. Given the lack of any resemblance of the sequence at the β-chain's C-terminus (Pro-Ala-Thr-Asp) to the canonical CAAX motif, it is not clear that the interactions seen by Park et al. reflect those made by authentic substrates. Nonetheless, Park et al. proposed that FPP would occupy the hydrophobic pocket in the center of the β-subunit barrel, while the peptide substrate would bind across the top of the barrel with its C-terminal carboxylate held in place by Lys164α, Arg291β, and Lys294β. As descibed above, the mutagenesis data implicate Arg291β in FPP binding and residues near Arg202β in peptide binding, and these proposals are consistent with our structural data.

Further structural work will be required if solutions to the remaining structure/function puzzles are to be found. As examples, the possible role of phosphorylation is not clear, the role of the Pro-rich sequence at the N-terminus of the α-subunit remains unknown, and the residues critical for catalysis have not all been identified. To begin to address

these questions and others, we have identified crystallization conditions at a pH more favorable for peptide binding, and further studies are in progress.

ACKNOWLEDGMENT

The authors thank David Waugh, Kwei Lan Tsao, Gerard Randolph, Yu-ching Pan, Hanspeter Michel, Doreen Ciolek, Kurt Hollfelder, Barbara De Barbieri, Marek Sochacki, and Vance Bell for help with protein expression, purification, and characterization; Vince Madison and Alex Wood for helpful discussions; Jim Marsters for the inhibitor BG168; and Guy James, Michael Brown, and Joseph Goldstein for the viral expression vectors.

REFERENCES

1. Gibbs, J. B., and Oliff, A. (1997) *Annu. Rev. Pharmacol. Toxicol. 37*, 143−166.
2. Park, H.-W., Boduluri, S. R., Moomaw, J. F., Casey, P. J., and Beese, L. S. (1997) *Science 275*, 1800−1804.
3. James, G. L., Goldstein, J. L., Brown, M. S., Rawson, T. E., Somers, T. C., McDowell, R. S., Crowlet, C. W., Lucas, B. K., Levinson, A. D., and Marsters, J. C., Jr. (1993) *Science 260*, 1937−1942.
4. Otwinowski, Z. (1994) in *Data Collection and Processing* (Sawyer, L., Isaacs, N., and Bailey, S., Eds.) pp 56−62, Science and Engineering Research Council, Daresbury Laboratory, Warrington, U.K.
5. Collaborative Computational Project, Number 4 (1994) *Acta Crystallogr. D50*, 760−763.
6. Kleywegt, G. J., and Jones, T. A. (1997) *Acta Crystallogr. D53*, 179−185.
7. Jones, T. A., Zou, J.-Y., Cowan, S. W., and Kjeldgaard, M. (1991) *Acta Crystallogr. A47*, 110−119.
8. de La Fortelle, E., and Bricogne, G. (1997) *Methods Enzymol. 276*, 472−494.
9. Murshudov, G. N., Vagin, A. A., and Dodson, E. J. (1997) *Acta Crystallogr. D53*, 240−255.
10. Brünger, A. T. (1992) *X-PLOR, Version 3.1: A System for X-ray Crystallography and NMR*, Yale University Press, New Haven, CT.
11. Laskowski, R., MacArthur, M., Moss, D., and Thornton, J. (1993) *J. Appl. Crystallogr. 26*, 91−97.
12. Hutchinson, E. G., and Thornton, J. M. (1996) *Protein Sci. 5*, 212−220.
13. Hooft, R. W. W., Vriend, G., Sander, C., and Abola, E. E. (1996) *Nature 381*, 272.
14. Reiss, Y., Goldstein, J. L., Seabra, M. C., Casey, P. J., and Brown, M. S. (1990) *Cell 62*, 81−88.
15. Kawabata, M., Imamura, T., Miyazono, K., Engel, M. E., and Moses, H. L. (1995) *J. Biol. Chem. 270*, 29628−29631.
16. Kumar, A., Beresini, M. H., Dhawan, P., and Mehta, K. D. (1996) *Biochem. Biophys. Res. Commun. 222*, 445−452.
17. Wang, T., Danielson, P. D., Li, B., Shah, P. C., Kim, S. D., and Donahoe, P. K. (1996) *Science 271*, 1120−1122.
18. Omer, C. A., Kral, A. M., Diehl, R. E., Prendergast, G. C., Powers, S., Allen, C. M., Gibbs, J. B., and Kohl, N. E. (1993) *Biochemistry 32*, 5167−5176.
19. Dolence, J. M., Rozema, D. B., and Poulter, C. D. (1997) *Biochemistry 36*, 9246−9252.
20. Furfine, E. S., Leban, J. J., Landavazo, A., Moomaw, J. F., and Casey, P. J. (1995) *Biochemistry 34*, 6857−6862.
21. Mathis, J. R., and Poulter, C. D. (1997) *Biochemistry 36*, 6367−6376.
22. Mitsuzawa, H., Esson, K., and Tamanoi, F. (1995) *Proc. Natl. Acad. Sci. U.S.A. 92*, 1704−1708.
23. Del Villar, K., Mitsuzawa, H., Yang, W., Sattler, I., and Tamanoi, F. (1997) *J. Biol. Chem. 272*, 680−687.
24. Trueblood, C. E., Boyartchuk, V. L., and Rine, J. (1997) *Proc. Natl. Acad. Sci. U.S.A. 94*, 10774−10779.
25. Qian, Y., Blaskovich, M. A., Saleem, M., Seong, C. M., Wathen, S. P., Hamilton, A. D., and Sebti, S. M. (1994) *J. Biol. Chem. 269*, 12410−12413.
26. Qian, Y., Vogt, A., Sebti, S. M., and Hamilton, A. D. (1996) *J. Med. Chem. 39*, 217−223.

BI980531O